Network dynamics of chalcogenide glasses. I. Germanium diselenide

U. Walter,* D. L. Price, S. Susman, and K. J. Volin
Materials Science Division and Intense Pulsed Neutron Source, Argonne National Laboratory, Argonne, Illinois 60439-4843
(Received 6 July 1987)

The scattering function $S(Q,E)$ of vitreous $GeSe_2$ at 13 K was measured with inelastic neutron scattering over a wide range of variables ($1<Q<8$ Å^{-1}, $0<E<45$ meV), with use of a chopper spectrometer at the Intense Pulsed Neutron Source. The data are analyzed in terms of the effective one-phonon density of states $G(E)$, the Q dependence of $S(Q,E)$ at different values of energy transfer E, and the elastic structure factor $S_{el}(Q)$. The data are discussed in terms of the normal modes of vibration of a $Ge(Se_{1/2})_4$ molecule. Certain features in the data can be unambiguously identified with such modes on the basis of the behavior of the dynamic structure factor $S(Q,E)$ at fixed E. Other features cannot be explained in this way and their understanding must await the development of a detailed microscopic model.

I. INTRODUCTION

Chalcogenide glasses provide excellent materials for investigating various aspects of the dynamics of the glassy state. Stable vitreous phases, with many possibilities for the component atoms, exist over a broad range of composition. Most of these can be readily prepared, by quenching from the melt, in the quantities required for inelastic neutron scattering. The present paper is devoted to vitreous $GeSe_2$, which appears to be an especially favorable compound for glass formation.[1] The following paper[2] describes a similar study on vitreous $SiSe_2$. Both $GeSe_2$ and $SiSe_2$ provide an interesting comparison with an earlier measurement on SiO_2.[3,4] While all three glasses have analogous AX_2 structures, built up by $A(X_{1/2})_4$ tetrahedra, the selenide glasses are distinguished from the oxide glass by smaller band gaps and heavier mass of the X atom. As discussed below, the latter has a profound impact on the dynamics of the network.

The structure of vitreous $GeSe_2$ has been measured with both x rays[5] and neutrons.[6–8] In contrast to SiO_2, for which all structural data can be interpreted on the basis of corner-shared SiO_4 tetrahedra, the $GeSe_2$ network appears to incorporate both corner-shared and edge-shared entities. This is also a basic feature of crystalline $GeSe_2$.[9] Another important, experimental difference is that Ge has a slightly higher scattering length than Se, and so the neutron scattering reflects in part the configuration and motion of the group-IV atom, in contrast to SiO_2 where the scattering is dominated by the O atoms.

II. EXPERIMENTAL PROCEDURES

Since the procedure used in these measurements was very similar to that used in the SiO_2 study,[4] only a very short outline of the neutron scattering formalism, spectrometer, and data-analysis procedure will be given here.

A. Neutron scattering formalism

The basic quantity measured in this experiment is the double differential cross section:[10]

$$\frac{d^2\sigma}{d\Omega\, dE}=\langle \bar{b}^2\rangle \frac{k_1}{k_0}\langle S(Q,E)\rangle \ , \tag{1}$$

where the symbols have the usual connotation and the angular brackets $\langle\ \rangle$ signify averages over the atoms in the sample. The average scattering function $\langle S(Q,E)\rangle$ appearing in Eq. (1) represents a combination of coherent and incoherent scattering. Since in both Ge and Se the incoherent fraction of the scattering cross section is quite small ($\simeq 5\%$), the scattering function of $GeSe_2$ is dominated by the coherent part:

$$S_c(Q,E)=\frac{1}{N\langle \bar{b}^2\rangle \hbar}\int_{-\infty}^{\infty}\sum_{i,i'}\bar{b}_i\bar{b}_{i'}\langle e^{-i\mathbf{Q}\cdot\mathbf{R}_i(0)}e^{i\mathbf{Q}\cdot\mathbf{R}_{i'}(t)}\rangle e^{-iEt/\hbar}dt \ . \tag{2}$$

Integration of Eq. (1) over E gives the static structure factor

$$S(Q)=\int_{-\infty}^{\infty}S_c(Q,E)dE$$
$$=\frac{1}{N\langle \bar{b}^2\rangle}\sum_{i,i'}\bar{b}_i\,\bar{b}_{i'}\langle e^{i\mathbf{Q}\cdot[\mathbf{R}_{i'}(0)-\mathbf{R}_i(0)]}\rangle \ , \tag{3}$$

which approaches 1 as $Q\rightarrow\infty$.

For a solid in which the atoms vibrate about well-defined equilibrium positions, and at wave vectors Q which are not too large, the scattering function can be expanded in terms of the orders of phonon scattering:[10]

$$S_c(Q,E)=S_{c,el}(Q,E)+S_{c,1}(Q,E)+S_{c,2}(Q,E)+\cdots \ . \tag{4}$$

The first term represents the elastic scattering:

 ©1988 The American Physical Society

$$S_{c,\mathrm{el}}(Q,E)=S_{\mathrm{el}}(Q)\delta(E)\ , \tag{5}$$

where the elastic structure factor is given by

$$S_{\mathrm{el}}(Q)=\frac{1}{N\langle \bar{b}^2\rangle}\sum_{i,i'}\bar{b}_i\bar{b}_{i'}e^{-(W_i+W_{i'})}e^{i\mathbf{Q}\cdot(\mathbf{i}'-\mathbf{i})}\ . \tag{6}$$

For an isotropic system the terms in the exponent of the Debye-Waller factor are

$$W_i(Q)=Q^2\langle u_i^2\rangle/6\ , \tag{7}$$

where $\langle u_i^2\rangle$ is the mean-square displacement of an atom i averaged over time.

The second term in Eq. (4) represents the one-phonon scattering, which at low temperatures ($kT\ll\hbar\omega_j$) is confined to the neutron-energy-loss side:

$$S_{c,+1}(Q,E)=\frac{1}{N\langle \bar{b}^2\rangle}\sum_{i,i'}\bar{b}_i\bar{b}_{i'}e^{-(W_i+W_{i'})}e^{i\mathbf{Q}\cdot(\mathbf{i}'-\mathbf{i})}\sum_j\hbar\frac{(\mathbf{Q}\cdot\mathbf{e}_i^j)^*(\mathbf{Q}\cdot\mathbf{e}_{i'}^j)}{2(M_iM_{i'})^{1/2}\omega_j}\langle n_j+1\rangle\delta(E-\hbar\omega_j)\ , \tag{8}$$

where the $\mathbf{e}_i^j$, ω_j, and $\langle n_j+1\rangle=[1-\exp(-\hbar\omega_j/kT)]^{-1}$ represent the displacement vector, frequency, and population factor of the normal mode j of the solid. The third and higher terms in Eq. (4) represent multiphonon scattering to which two or more normal modes contribute simultaneously. These generally introduce a relatively smooth and, at low temperatures and moderate values of Q, low background under the one-phonon scattering.

Finally, it is convenient to define a generalized density of states $G(Q,E)$ by the relation

$$S_{c,+1}(Q,E)=e^{-2\overline{W}}\frac{\hbar^2Q^2}{2\overline{M}E}\langle n+1\rangle G(Q,E)\ , \tag{9}$$

where

$$2\overline{W}=Q^2\overline{\langle u^2\rangle}/3 \tag{10}$$

is the average of the mean-square displacements taken over all atoms in the sample and $\overline{M}^{-1}=\sum_i M_i^{-1}/N$. If the incoherent approximation is assumed to apply, i.e., the phase factors in Eq. (8) are assumed to average to zero for $i\neq i'$, and if in addition the other factors can be averaged independently, $G(Q,E)$ reduces to $Z(E)$, the one-phonon density of states (see Ref. 4 for a more-detailed discussion). In the case of a solid with more than one type of atom, this situation does not hold, even for incoherently scattering nuclei. Nevertheless, it may be useful to derive an *effective* density of states by averaging $G(Q,E)$ over an extended range of Q, and consider this as a rough approximation to the true density of states $Z(E)$.

B. Sample preparation

Considerable attention has been given to the preparation and characterization of vitreous germanium selenide for these and other experiments. We have observed the effect of both homovalent and heterovalent anion impurities (such as oxide and hydride) upon the short-range order (SRO, 3–5 Å) and the intermediate-range order (IRO 5–15 Å) of the system. Equally important are deviations from exact stoichiometry (which can be best determined by *in situ* optical spectroscopies). This section contains a brief outline of the procedures used for preparing the samples of the size ($\simeq$125 g) required for inelastic neutron scattering. A full description will be contained in a forthcoming publication.[8] Homovalent oxide impurity changes the local structural unit and alters the SRO by distorting the symmetry of the $Ge(Se_{1/2})_4$ tetrahedron. It modifies the IRO by perturbing the intertetrahedral angle between corner-shared tetrahedra. It further changes the IRO by its refusal to enter into edge bonding between tetrahedra. Aleovalent hydride impurity creates dangling bonds (which it then saturates) and breaks the connectivity of the network. The effects on both the phonon and electron density of states can be significant—even at relatively low concentrations. The sad condition of the thermodynamics literature on c-$GeSe_2$ (Ref. 11) (and other crystalline binary chalcogenides) is tangible evidence of the seriousness of the impurity problem.

Semiconductor-grade germanium and ultrahigh-purity selenium were the starting materials for glass synthesis. They were purified to remove anion contamination from the surface and from the bulk.[8] Stoichiometric quantities of the reactants were loaded into 10-mm-o.d. fused silica tubes in 20-g batches. Acid pretreatment and high-temperature vacuum bakeout of the tubes were performed to minimize the Si-O and Ge-O contamination of the melt. The melt was homogenized in a rocking furnace, and the vacuum-sealed ampoules were quenched into a 10 mass % $NaOH$-H_2O bath. The glass ingot, which could slip about inside the ampoule, was relaxed at 300 °C—a temperature below the range where phase separation or crystallization occurs.[12]

The resultant $GeSe_2$ glass samples were extensively characterized for stoichiometry, purity, crystallinity, and homogeneity by chemical analyses, Raman scattering, infrared absorption spectrometry, optical microscopy (polarized transmission and infrared transmission), and differential thermal analyses. Possible concentration fluctuations at the nanostructure length scale (15–100 Å) have yet to be evaluated by analytical electron microscopy.

Figure 1 shows the infrared transmission spectrum of a-$GeSe_2$ prepared without completely appropriate purification and outgassing procedures. The Ge-O stretching band at 800 cm^{-1} in curve a represents 30 ppm W oxygen contamination in the glass. Curve b is typical of the $GeSe_2$ glass used in the present work and contains <9 ppm W oxygen. Curiously, the various purification routines that are most effective in removing oxygen often introduce a small but measurable concentration of hydrogen.[8] This appears as the –Se–H

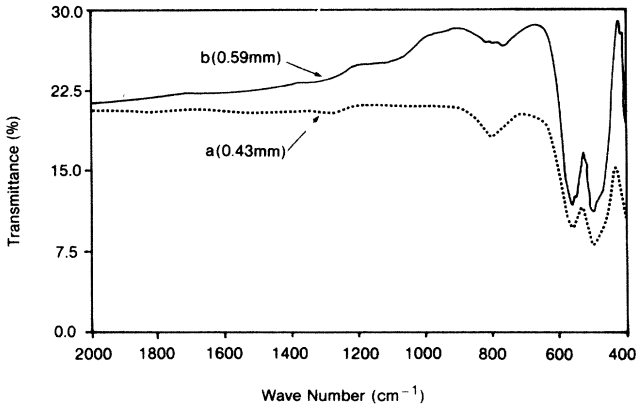

FIG. 1. Oxygen content of a-$GeSe_2$ as measured by FTIR absorption spectrometry. (a) 30 ppm W oxygen; $A(800\ \text{cm}^{-1})=2.76\ \text{cm}^{-1}$; (b) <9 ppm W oxygen, $A(800\ \text{cm}^{-1})=0.95\ \text{cm}^{-1}$.

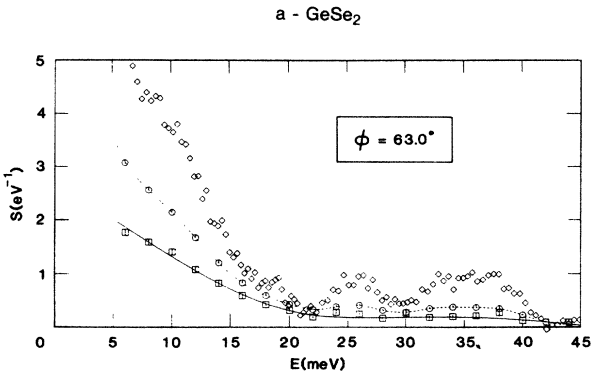

FIG. 2. Example of the experimental data for $S(Q,E)$ at a scattering angle $\phi=63.0°$. The solid and dashed lines show the multiple and single scattering calculated in the Monte Carlo simulation of the experiment described in the text. The data as shown by the diamonds have been corrected for the effects of multiple scattering and self-shielding in the sample.

stretching frequency at 2240 cm^{-1} and not as –O–H or H–O–H. The chemistry involved is not understood but is under investigation.

C. Neutron measurements

The measurements were carried out at the Low-Resolution Medium-Energy Chopper Spectrometer[13] at the Intense Pulsed Neutron Source at Argonne National Laboratory. This is a direct-geometry instrument in which the incident energy is kept fixed and the scattered neutron energies measured in a multiangle array of detectors around the sample. Data may therefore be collected simultaneously over an extended range of (Q,E) space.

The sample was positioned in transmission geometry at 45° to the incident beam, and the measurements were carried out with an incident energy of 60.06 meV. Data were analyzed independently in 41 groups of detectors with scattering angles ϕ ranging continuously from 2.7° to 116.0°. The $GeSe_2$ sample, consisting of grains 1–5 mm in diameter with a total weight of 127.5 g, was contained in a thin aluminum foil pan of dimensions $75\times100\times6.8$ mm. This assembly was mounted in a copper frame suspended from a Displex refrigerator; the frame was covered with a cadmium mask. The sample temperature as measured with a thermocouple attached to the Cu frame was 13±2 K. Runs were made with (a) the $GeSe_2$ sample (129 h), (b) a vanadium reference 2.825 mm thick (32 h), (c) a Cd absorber (41 h), and (d) no sample (105 h), inside the Al foil. Transmissions T of the $GeSe_2$ sample and V reference derived from integrated beam monitor counts were 0.740 and 0.825, respectively. Composite background runs (e) defined by

$$S^{(e)}=TS^{(d)}+(1-T)S^{(c)} \tag{11}$$

were subtracted from the $GeSe_2$ and V runs, where T is the appropriate measured transmission. The numbers of formula units in the beam were estimated as 0.333 and 1.023×10^{24} for the $GeSe_2$ and V, respectively. Using standard procedures,[4,13] the corrected V data were used to obtain normalized $S(\phi,E)$ data for the $GeSe_2$ sample.

D. Data analysis

The Monte Carlo program[14] MSCAT was used to calculate the multiple-scattering correction to the data, with the same procedure as that used for SiO_2.[3,4] For the model used in the Monte Carlo simulation, additional data had to be supplied: the incoherent inelastic cross section, derived from a density of states $Z(E)$ obtained by calculating $G(Q,E)$ from the uncorrected $S(Q,E)$ data and averaging it over the Q range of the measurement; the Debye-Waller factor, which was taken as $\exp(-Q^2\langle u^2\rangle/3)$ [see Eq. (10)] where $\langle u^2\rangle/3$ was calculated from $Z(E)$ to have the value 0.002 57 Å^2; and the elastic scattering, assumed to be given by

$$S_{\text{el}}(Q)=S(Q)-1+e^{-Q^2\langle u^2\rangle/3}, \tag{12}$$

where $S(Q)$ was obtained from the diffraction data of Ref. 8. Equation (12) ensures that the total model scattering function—elastic plus incoherent inelastic—integrates to $S(Q)$. The Monte Carlo simulation was carried out for 100 000 events. The calculated multiple-scattering component was then subtracted from the measured $S(\phi,E)$, and a correction for the self-shielding of the sample was also applied.

Figure 2 shows a comparison of the single and multiple scattering from the Monte Carlo simulation with the *corrected* experimental $S(\phi,E)$ data for a typical ϕ, 63.0°; the elastic region has been suppressed in order to show up the inelastic scattering. It can be seen that at this intermediate angle the multiple scattering contributes about 40% of the inelastic scattering; the fraction is higher at low angles and lower at high angles.

The $S(\phi,E)$ data were interpolated onto constant Q using a spline interpolation,[15] thus providing $S(Q,E)$ over the (Q,E) range of the measurements: $0.6<Q<8.5$ Å^{-1} (at $E=0$) and $-5<E<55$ meV. $G(Q,E)$ was obtained by means of Eqs. (9) and (10), using $\langle u^2\rangle/3=0.002\,57$ Å^2, and averaged over the Q range 2.0–7.5 Å^{-1} to obtain an initial estimate for the effective density of states. Fi-

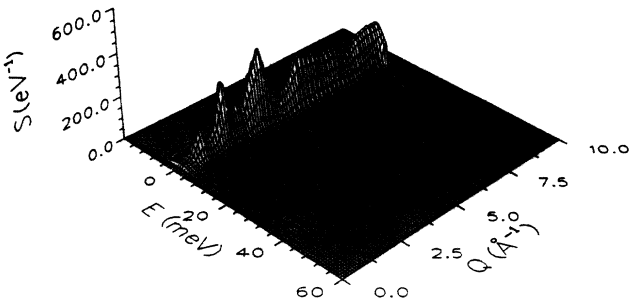

FIG. 3. Corrected $S(Q,E)$

nally, the multiphonon component of $G(Q,E)$ was calculated (again within the incoherent approximation) using an iterative procedure,[4] and subtracted from the data to yield a "one-phonon" effective density of states $G(Q,E)$.

III. RESULTS AND DISCUSSION

An overview of the measured $S(Q,E)$ is given by the three-dimensional plots in Figs. 3 and 4. The total scattering, shown in Fig. 3, is dominated by the elastic scattering, with the Q dependence represented by the structure factor $S(Q)$ and the energy broadening by the instrumental resolution; this is discussed in Sec. III A below. Figure 4 shows the same region of (Q,E) space with the elastic region suppressed in order to exhibit the inelastic scattering. Structure along both Q and E directions can be clearly observed. This is discussed in detail in Secs. III B and III C.

A. Elastic and total scattering

The total scattering function $S(Q)$ was estimated by integrating the measured scattering function $S(Q,E)$ over the energy interval -5 to $+45$ meV, containing most of the inelastic scattering at this low temperature. The result is shown in Fig. 5 in comparison with the diffraction result from Ref. 8. The agreement is reasonably good, considering the coarser spacing of detectors in the LRMECS measurement. No normalization was applied

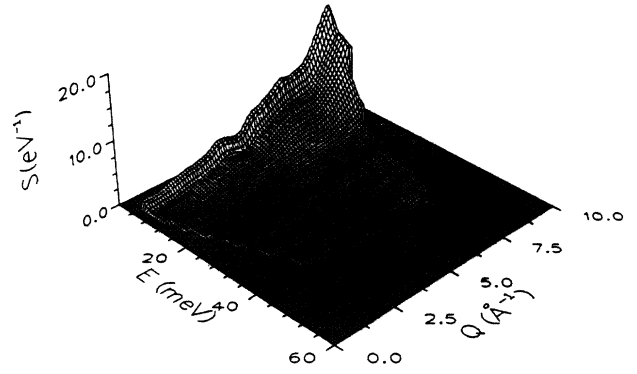

FIG. 4. Same as Fig. 3 but with the elastic region suppressed to highlight the inelastic scattering. (Note the factor 30 difference in scale.)

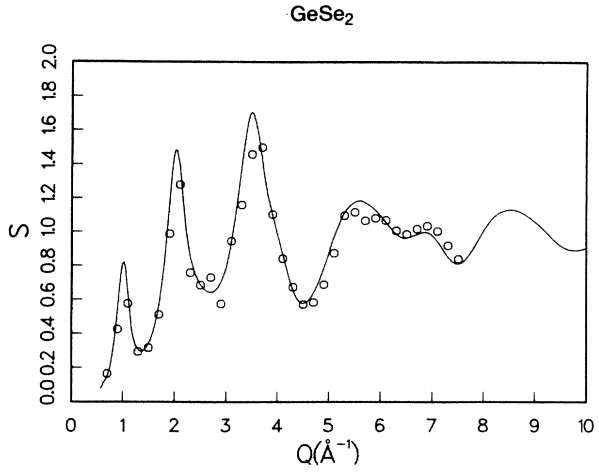

FIG. 5. $S(Q)$ derived from integration of $S(Q,E)$ from this experiment (○) with that measured in a diffraction experiment (Ref. 8) (——).

in making this comparison, i.e., the scattering function appears to be correctly normalized on an absolute basis as a result of the experimental procedures followed (Sec. II C). The Q dependence in the comparison provides an additional check on the validity of the multiple-scattering and self-shielding corrections.

More interesting is the elastic scattering function $S_{el}(Q)$, estimated by integrating the measured scattering function over the more restricted region -5 to $+5$ meV, sufficient to span the resolution function centered at $E=0$. Figure 6 shows the result plotted in two ways: (a) in the form $\ln[S_{el}(Q)/S(Q)]$ and (b) in the form $\ln[S_{el}(Q)-S(Q)+1]$, both against Q^2. As discussed[4] in connection with SiO_2, (a) should exhibit structure in phase with $S(Q)$ while (b) should follow the self-scattering [see also Eq. (12)]:

$$\overline{\exp(-2W)}=\frac{1}{N\langle\bar{b}^2\rangle}\sum_i \bar{b}_i^2\exp(-2W_i) \tag{13}$$

with W_i given by Eq. (7), as long as thermal vibrations between different atoms are uncorrelated. Figure 6 shows that this function is fitted reasonably well by a straight line corresponding to a mean Debye-Waller factor $\exp(-Q^2\langle u^2\rangle/3)$ with $\langle u^2\rangle/3=0.00188$ Å^2, indicating that, as in SiO_2, the correlations between thermal vibrations on different atoms are relatively small.

The value of $\langle u^2\rangle/3$ obtained from Fig. 6 is 27% smaller than that calculated from the density of states (see Sec. II D). The discrepancy may be caused by the fact that the latter is not measured accurately at low energies due to the difficulty in subtracting the resolution-broadened elastic peak, and this region contributes significantly to $\langle u^2\rangle$. Another comparison may be made with the Debye-Waller factor for pair correlations derived from the interference function measured in a diffraction experiment,[8] which gives $\langle u^2\rangle/3=0.0014$ Å^2 at 10 K. Again, this comparison is only meaningful if correlations between vibrations on different atoms can be neglected.

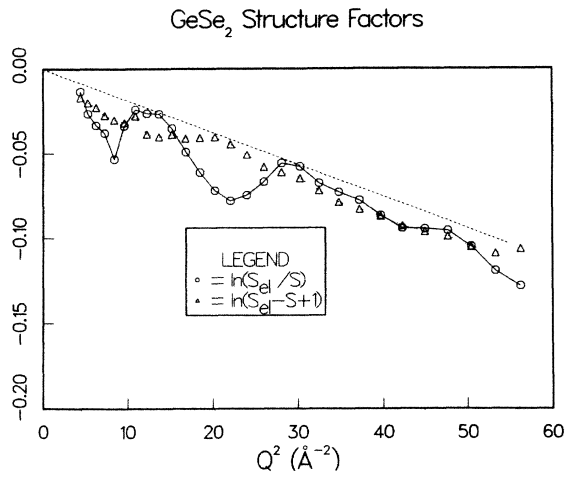

FIG. 6. Structure factors for $GeSe_2$ plotted against Q^2: $\ln[S_{el}(Q)/S(Q)]$ (——); $\ln[S_{el}(Q)-S(Q)+1]$ (· · · ·); $-\alpha Q^2$ with $\alpha=0.001\,88$ Å^2 (— — —).

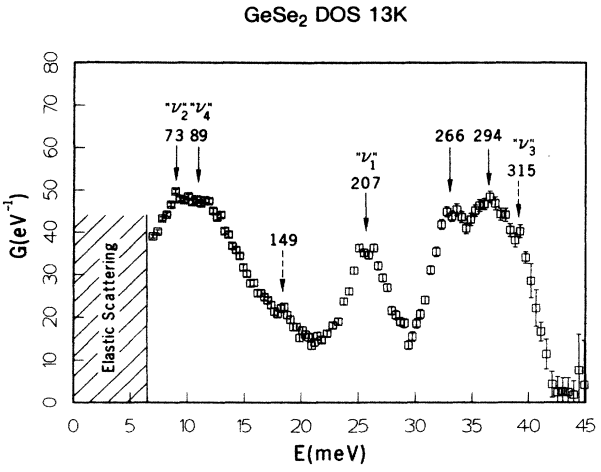

FIG .7. One-phonon effective density of states $G(E)$; the labels attached to features in $G(E)$ give the frequency in cm^{-1} and, where appropriate, assignments discussed in the text in terms of modes of a $Ge(Se_{1/2})_4$ tetrahedron.

B. Effective density of states

The one-phonon effective density of states $G(E)$ obtained with the procedure described in Sec. II A is shown in Fig. 7. As discussed in Sec. II A, $G(E)$ is not identical to the true density of states $Z(E)$, but it should be reasonably close to it for the case of $GeSe_2$, since the masses and scattering lengths of the two component elements are quite similar. As discussed above, the correct form of the function was difficult to obtain at small E and this region is omitted from the plot. The density of states is dominated by five peaks centered approximately at energies of 9, 11, 25.7, 33, and 36.5 meV, respectively (1 meV $\simeq 8.0655$ cm^{-1}). In terms of wave numbers, for comparison with the optical spectroscopy literature, these correspond to 73, 89, 207, 266, and 295 cm^{-1}, as indicated on Fig. 7. The peak at 25.7 meV may have some structure and, indeed, corresponds to the celebrated A_1 tetrahedral mode which, along with its "companion" line, has been the subject of extensive study and controversy in Raman studies of vitreous $GeSe_2$.[7,16–18] In addition to the five main peaks, there are weaker features in the spectrum around 18.5 and 39 meV (149 and 315 cm^{-1}), which appear to be real and not experimental artifacts.

Table I compares the energies of the neutron peaks with those observed in some of the Raman (Refs. 16 and 17) and ir (Ref. 18) spectroscopic studies in the literature. The entries in a given row simply represent peaks observed in a similar energy interval, which may or may not represent the same physical feature. The assignments given by the different authors are shown in the right-hand part of the table.

There are excellent grounds for believing that a-$GeSe_2$ consists principally of $Ge(Se_{1/2})_4$ tetrahedra, with both edge-sharing and corner-sharing configurations present. In the crystal,[9] 25% of the Se atoms are involved in edge sharing and 75% in corner sharing. A similar proportion in the glass is indicated by both x-ray[5] and neutron[7,8] diffraction results, and also inferred from Raman scattering data.[16]

TABLE I. Neutron and optical peaks in density of states of a-$GeSe_2$. (Question marks indicate uncertain values.)

Measured frequencies (cm^{-1})					Assignment[a]			
Neutron (present work)	Raman (Ref. 16)	Raman (Ref. 17)	ir (Ref. 18)	$GeBr_4$ (Ref. 19)	(Ref. 16)	(Ref. 17)	(Ref. 18)	$GeBr_4$ (Ref. 19)
73		82	80	78		E	E	$\nu_2(E)$
89			100	111			F_2	$\nu_4(F_2)$
149?	140	135						
	179	175				Ge_2		
207	201	198	200	234	A_1	A_1	A_1	$\nu_1(A_1)$
	218	212			A_1^*	Se_2		
266	240	257	255			F_2+Ge_2	F_2	
	270							
294								
315?	310	304		328		F_2		$\nu_3(F_2)$

[a]Symbols other than conventional symmetry designations have the following meaning: A_1^*: A_1 mode of edge-sharing tetrahedra; Ge_2: $Ge_2(Se_{1/2})_6$ units; Se_2: dimerized Se-Se units.

According to an idea proposed originally by Sen and Thorpe,[20] the dynamics of tetrahedrally coordinated AX_2 glasses may be qualitatively understood in terms of the bond angle θ at the X atom. If $\theta \simeq 90°$, the vibrations of each $A(X_{1/2})_4$ tetrahedron are effectively decoupled and the vibrational spectrum resembles that of an isolated tetrahedron. For larger (or smaller) values of θ, in particular those exceeding a critical angle $\theta_c = \cos^{-1}(2M_X/3M_A)$, the coupling intensifies and it becomes more meaningful to treat the $X(A_{1/4})_2$ unit as the starting approximation. This picture appears to provide a reasonable description of the higher-energy modes of SiO_2.[3,21] In the $GeSe_2$ crystal, the average values of θ are 80.4° for edge sharing and 98.0° for corner sharing, both quite close to 90° and considerably less than $\theta_c = 136.5°$; the values in the glass appear to be similar. The isolated tetrahedron picture should therefore give a good first approximation. The fifth column in Table I shows the four fundamental frequencies of the tetrahedral molecule[19] that is the closest analog to $GeSe_2$, namely, $GeBr_4$. Modes similar to these frequencies are observed in the optical spectra of both β- and a-$GeSe_2$ and assigned with a reasonable degree of confidence. The exception is the higher-frequency F_2 mode which has been assigned to either the 250–260- or the 300–310-cm^{-1} regions of the spectrum. As discussed earlier, the A_1 mode is split into fundamental and "companion" lines, assigned in Refs. 7 and 16 to corner-sharing and edge-sharing configurations.

The neutron spectrum shown in Fig. 7 shows features which can be quite reasonably associated with the four tetrahedral modes, as labeled in the figure. Some supporting evidence for this comes from consideration of the dynamic structure factors, as discussed in the next subsection. This leaves the feature at 266 and 294 cm^{-1} and the possible one at 149 cm^{-1} to be explained. Bridenbaugh *et al.*[17] associate features at 175 and 257 with vibrations of an ethanelike $Ge_2(Se_{1/2})_6$ unit; this interpretation is consistent with Raman measurements on the Ge-rich side of $GeSe_2$ by Kumagai *et al.*,[18] in which modes at 175 and 265 cm^{-1} intensify with increasing Ge concentration. The question must be considered unresolved at the present time. The strong peak at 294 cm^{-1} in the neutron spectrum does not connect with any of the optical features.

C. Dynamic structure factors

The Q dependence of the scattering function in Eq. (8) at a given value of E, which arises from the polarization vectors e_i^j describing the atomic displacements in the modes contributing at that value of E, provides, in principle, a means for identifying the features in the density of states measured with inelastic neutron scattering. Such an identification has been successful in the case of the elemental amorphous solid a-Ge,[22] but less so in the case of the compound glass SiO_2.[3] In the case of $GeSe_2$, the explanation of features in the optical spectra on the basis of a tetrahedral model, as discussed in the last section, suggests the calculation of the dynamic structure factors from this model to compare with those observed experimentally.

The vibrations of tetrahedral pentatomic molecules were treated in some detail by Rosenthal[23] over 50 years ago. In particular, she calculated the normal coordinates for the vibrations and set up the equations of motion in terms of these coordinates. From these it is straightforward to calculate the polarization vectors of each of the five atoms in each mode and calculate the dynamic structure factor for each mode according to Eq. (8), taking the appropriate degeneracies into account. The force model used was the valence-force model which, with only two parameters, gives a reasonable representation of the normal modes of tetrahedral molecules.[19] The values used for the two parameters in the present calculation were $f_1''' = 188$ and $f_2''' = 24$ kdyn/cm, giving frequency values of ν_1, ν_2, ν_3 and $\nu_4 = 201$, 62, 322, and 73 cm^{-1}, respectively, quite close to the experimental values assigned in Table I. In any case, the polarization vectors for modes ν_1 and ν_2 do not depend on the forces, and those for ν_3 and ν_4 (which are coupled modes) do so only weakly.

Figures 8–10 show the experimental structure factors measured at three energies corresponding to those as-

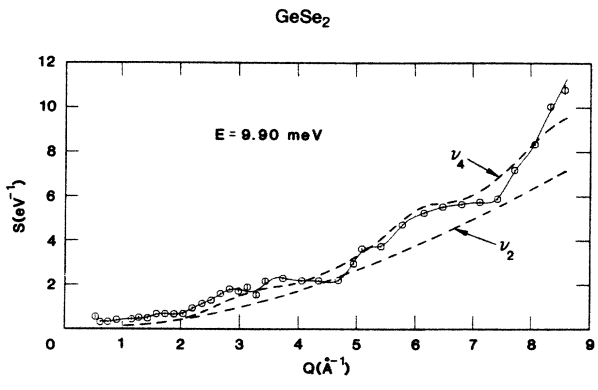

FIG. 8. The dynamic structure factor $S(Q,E)$ measured around $E = 9.9$ meV (○) (80 cm^{-1}); the solid curve passing near the data points represents a smoothed cubic spline fit to the data. The dashed curves marked ν_2 and ν_4 represent calculations based on $Ge(Se_{1/2})$ tetrahedra.

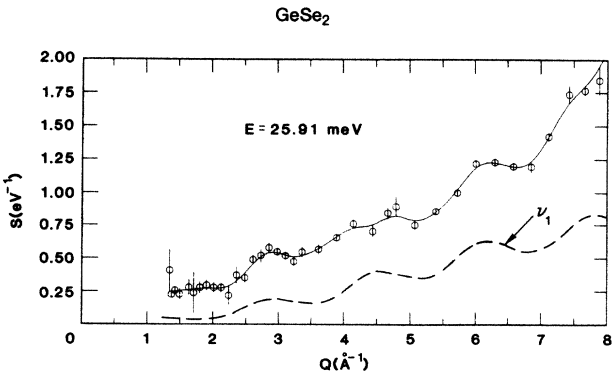

FIG. 9. $S(Q,E)$ measured around $E = 25.9$ meV (209 cm^{-1}); notation as for Fig. 7.

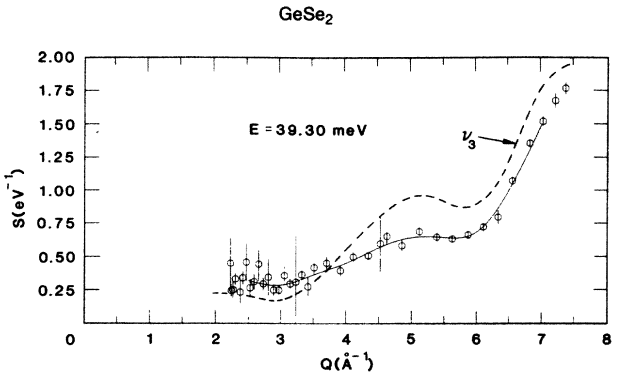

FIG. 10. $S(Q,E)$ measured around $E=39.3$ meV (317 cm^{-1}); notation as for Fig. 7.

signed to tetrahedral vibrations in Table I. Since the assigned frequencies for the ν_2 and ν_4 modes are closer than the energy resolution of this experiment ($\Delta E \simeq 4$ meV, or 32 cm^{-1}), the structure factors measured at these frequencies are quite similar, and both would be expected to contain contributions from both modes. Figure 8 therefore shows the experimental structure factor at the mean energy, 9.9 meV (80 cm^{-1}), and the comparison with the structure factors calculated for both ν_2 and ν_4. The other two modes should be well resolved and Figs. 9 and 10 show their structure factors measured at 25.9 and 39.3 meV (209 and 317 cm^{-1}) in comparison with the calculated factors for ν_1 and ν_3, respectively. Since the peaks calculated for the tetrahedral molecule are δ functions in energy while the experimental data represent averages over the resolution width ΔE, the calculated structure factors have been divided by $\Delta E=4.0$ meV for direct comparison with experiment. Apart from this factor there is no further normalization, i.e., *both experimental and calculated factors in Figs. 8–10 are absolutely and independently normalized.*

It is evident from Figs. 8–10 that the structure factors calculated for the ν_1, ν_3, and ν_4 modes reproduce the features in the measured factors remarkably well. It is possible that the ν_2 structure factor is also contributing in the region around 10 meV, but that is difficult to tell since it is so featureless. Also, while the amplitudes in the oscillations of $S(Q)$ for the ν_1 mode are similar to those calculated, they appear to be superimposed on a smooth, rising background. The reason for this is not understood; it is possible that other modes are contributing to this peak, since this mode has the lowest multiplicity (1) in the tetrahedral model. A higher resolution measurement might also shed light on this question. *Overall, the high degree of agreement confirms the assignments of the features in the spectrum with modes of the tetrahedral molecule, without any model-dependent assumptions.*

The following conclusions could be drawn from the experimental structure factors for other values of E, not displayed here.

(1) The structure factor at 18.1 meV (146 cm^{-1}) cannot be identified with any of those calculated for the tetrahedral molecule. In principle, it could be compared with that of a $Ge_2(Se_{1/2})_6$ molecule, but this did not seem justified in view of the weakness of this feature in the neutron spectrum and the uncertainty about this identification.

(2) The structure factors measured at 33.0 and 36.2 meV (266 and 292 cm^{-1}) are very similar to that at 39.3 meV, suggesting that these features are also associated with vibrations with ν_3 character.

IV. CONCLUSIONS

The structure factor of vitreous $GeSe_2$ measured by inelastic scattering of 60-meV neutrons gives a general confirmation of the picture of the dynamics which has been obtained by Raman and infrared spectroscopy over the past ten years. Features associated with three of the four fundamental modes of the $Ge(Se_{1/2})_4$ molecule are unambiguously identified by comparing the structure factors calculated for those modes with those measured experimentally. A feature observed in optical work in the region of 140–170 cm^{-1} appears in the neutron spectrum but too weakly to permit an analysis on the basis of the structure factor. The neutron spectrum shows considerable structure in the modes around 300 cm^{-1} associated with the tetrahedral ν_3 vibration. This is similar in appearance to the splitting observed in SiO_2 (Ref. 3) and is at present unexplained. It is hoped that light will be shed on these and other remaining questions about the dynamics of this glass by computer-simulation experiments now underway at Argonne National Laboratory.[24]

The total and elastic structure factors derived from the inelastic data are consistent with previous diffraction experiments and a mean-square thermal displacement $\langle u^2\rangle/3=0.001\,88$ Å^2. They indicate that correlations between the thermal displacements on neighboring atoms are negligibly small.

ACKNOWLEDGMENTS

The experimental measurements were carried out at the Intense Pulsed Neutron Source (IPNS) at Argonne National Laboratory, and the assistance of the IPNS Operations Staff is gratefully acknowledged. We have benefited from discussions with I. Ebbsjö, R. Kalia, C.-K. Loong, P. Vashishta, and A. C. Wright. Work supported by the U.S. Department of Energy (Basic Energy Sciences Program, Division of Materials Sciences), under Contract No. W-31-109-ENG-38.

*Present address: Department of Physics, University of California, Berkeley, CA 94720.

[1]J. C. Phillips, J. Non-Cryst. Solids **34**, 153 (1979).

[2]M. Arai, D. L. Price, S. Susman, K. J. Volin, and U. Walter, following paper, Phys. Rev. B **37**, 4240 (1988).

[3]J. M. Carpenter and D. L. Price, Phys. Rev. Lett. **54**, 441 (1985).

[4]D. L. Price and J. M. Carpenter, J. Non-Cryst. Solids **92**, 153

(1987).
[5]A. Feltz, M. Pohle, H. Steile, and G. Helms, J. Non-Cryst. Solids **69**, 271 (1985).
[6]O. Uemura, Y. Sagara, and T. Satow, Phys. Status Solidi A **32**, K91 (1975); O. Uemura, Y. Sagara, D. Muno, and T. Satow, J. Non-Cryst. Solids **30**, 155 (1978).
[7]R. J. Nemanich, F. L. Galeener, J. C. Mikkelsen, G. A. N. Connell, G. Etherington, A. C. Wright, and R. N. Sinclair, Physica B + C **117-118B**, 959 (1983).
[8]S. Susman, D. G. Montague, D. L. Price, and K. J. Volin (unpublished).
[9]Von G. Dittmar and H. Schäfer, Acta Crystallogr. Sect. B **32**, 2726 (1976).
[10]See, for example, D. L. Price and K. Sköld, in *Neutron Scattering*, edited by K. Sköld and D. L. Price (Academic, Orlando, 1986), p. 1.
[11]P. A. G. O'Hare, J. Chem. Thermodynamics **19**, 675 (1987).
[12]R. Azoulay, H. Thibierge, and A. Brenac, J. Non-Cryst. Solids **18**, 33 (1975).
[13]D. L. Price, J. M. Carpenter, C. A. Pelizzari, S. K. Sinha, I. Bresof, and G. E. Ostrowski, Argonne National Laboratory, Report No. ANL-82-80, 1982 (unpublished), p. 207.
[14]J. R. D. Copley, Comp. Phys. Commun. **7**, 289 (1974); **9**, 59 (1975); **9**, 64 (1975); **21**, 431 (1981); J. R. D. Copley, P. Verkerk, A. A. Van Well, and H. Fredrikse, *ibid.* **40**, 337 (1986); D. L. Price (unpublished).
[15]C. K. Loong and D. L. Price (unpublished).
[16]S. Sugai, Phys. Rev. B **35**, 1345 (1987); also contains a comprehensive list of references to previous work.
[17]P. M. Bridenbaugh, G. P. Espinosa, J. E. Griffiths, J. C. Phillips, and J. P. Remeika, Phys. Rev. B **20**, 4140 (1979).
[18]N. Kumagai, J. Shirafuji, and Y. Inuishi, J. Phys. Soc. Jpn. **42**, 1262 (1977).
[19]G. Herzberg, *Infrared and Raman Spectra of Polyatomic Molecules* (Van Nostrand, New York, 1945).
[20]P. N. Sen and M. F. Thorpe, Phys. Rev. B **15**, 4030 (1977).
[21]F. L. Galeener, A. J. Leadbetter, and M. W. Stringfellow, Phys. Rev. B **27**, 1052 (1983).
[22]N. Maley, J. S. Lannin, and D. L. Price, Phys. Rev. Lett. **56**, 1720 (1986).
[23]J. E. Rosenthal, Phys. Rev. **45**, 538 (1934); **46**, 730 (1934); **49**, 535 (1936).
[24]P. Vashishta, R. Kalia, and I. Ebbsjö (unpublished).

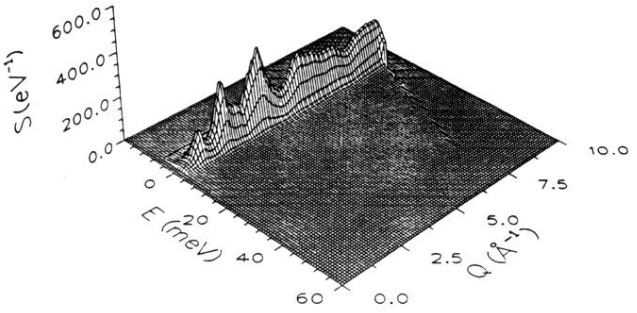

FIG. 3. Corrected $S(Q,E)$

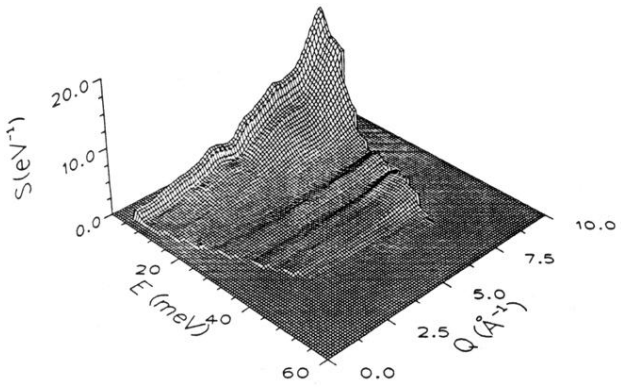

FIG. 4. Same as Fig. 3 but with the elastic region suppressed to highlight the inelastic scattering. (Note the factor 30 difference in scale.)